A Pseudospectral Method for Real-Time Motion Planning and Obstacle Avoidance

L.R. Lewis and I.M. Ross
Department of Mechanical and Astronautical Engineering
Naval Postgraduate School, Monterey, CA 93943
USA

IMROSS@nps.edu

ABSTRACT

In recent years, pseudospectral (PS) methods have been successfully applied to solve a rich number of trajectory optimization problems arising in aerospace application. Motivated by the success of this approach, we consider the problem of generating minimum-time trajectories for unmanned ground vehicles. Shapes of arbitrary number, size and configuration are modelled in the form of path constraints in the resulting optimal control problem formulation. PS methods are used to solve the constrained, nonlinear optimal control problem. Solutions are obtained within a few seconds even under a MATLAB environment running on legacy computer hardware. A complete problem formulation is developed including a derivation of the necessary conditions for optimality. The trajectories are mathematical extremals as they satisfy all the optimality conditions. What is noteworthy about our approach is that the difficulties associated in solving the Hamiltonian equations are completely circumvented by an application of the Covector Mapping Theorem. Solved examples are provide to illustrate the tools and techniques.

1.0 INTRODUCTION

Trajectory planning occurs within the guidance system of every autonomous or semi-autonomous vehicle, whether it is the $300 Roomba® or the $300M New Horizons spacecraft. Trajectory planning allows the vehicle to travel from one location to another safely, within the limits of its electrical and mechanical capabilities, and in some situations, in an optimal manner with respect to use of fuel, expenditure of time, or distance travelled. The development of autonomous trajectory planning technologies has been painstakingly slow; the variety of tasks accomplished by every five-year-old human cannot, at this point in time, be replicated by a multi-million dollar robot. The advantages, however, to accomplishing human-like tasking with a robot are immeasurable and for that reason continue to be a goal of researchers everywhere.

1.1 Motivation

A broad class of problems are emerging that implore the ability to remove the human from the control loop. The rewards of robotic systems are increased production, reliability, safety, and capability. Spacecraft assembly and repair, space station replenishment, and certain facets of planetary exploration were viewed solely as human missions during the Apollo and early Space Shuttle periods. Ever improving technologies and capabilities and cost and risk reduction have been the driving forces in reshaping these paradigms; now, systems are either being developed or have already been fielded to accomplish these tasks unmanned. The

Lewis, L.R.; Ross, I.M. (2007) A Pseudospectral Method for Real-Time Motion Planning and Obstacle Avoidance. In *Platform Innovations and System Integration for Unmanned Air, Land and Sea Vehicles (AVT-SCI Joint Symposium)* (pp. 10-1 – 10-22). Meeting Proceedings RTO-MP-AVT-146, Paper 10. Neuilly-sur-Seine, France: RTO. Available from: http://www.rto.nato.int/abstracts.asp.

Mars rovers Spirit and Opportunity are shining examples of the utilization of robotic technologies to aid human exploration, accomplishing tasks that could not be achieved otherwise. The applications of trajectory planning are not limited to systems outside the Earth's atmosphere. Military applications of unmanned and autonomous vehicles have drawn considerable interest and recognition in recent years. Most notable is the Unmanned Aerial Vehicle (UAV), but considerable advances are making the incorporation of unmanned ground (UGV) and sea surface vehicles possible. Meanwhile, new classes of UAVs are under development that are carried by soldiers on the ground, deployed only when operationally needed, and implemented without the overhead of the larger current systems. These systems remove humans from jobs that would be otherwise extremely dangerous. Moving away from the public sector, the private arena is the ultimate stage for technological utility. While the future possibilities are truly endless, robotic technologies are already improving consumer lives by eliminating such tedious tasks as vacuuming and parallel parking.

1.2 Background

The various applications of trajectory planning led to the evolution of differing techniques to solve their problems. Aeronautical and space applications drove the development of nonlinear optimal control techniques and continue to do so [1-6]. In these situations, global problem knowledge is assumed, vehicle motion is precisely understood, few physical constraints obstruct the vehicular motion, and trajectory optimization is key to design and mission success. Robotics applications propelled a differing solution, but it was a solution better adapted to fit the inherent situational complexities including: limited problem knowledge, noisy sensors, uncertain dynamical characteristics, intricate obstacle-rich environments, limited computational power, and the necessity to generate feasible solutions. Despite the general similarity between problems, these two fields of application experienced little cross-pollinization. Aerospace applications desired optimality and robotics applications desired simplicity and an ability to handle uncertainty.

Many techniques fall within the realm of robotics-based trajectory planning [7-8]. Potential functions were first developed over thirty years ago [9], and though they can be simplistic, they are still used in many functions today [10-11]. In general, this approach can be used successfully in the presence of uncertainty but it suffers from occurrences of local minima, a lack of trajectory optimality, and difficulty in accommodating complex vehicle constraints [12]. More recent developments place heavy emphasis on sampling-based planning techniques. Notably, sampling methods include Probabilistic Road Maps (PRM), Rapidly-Exploring Random Trees (RRT), and Expansive Space Trees (EST) to name a few [8, 13-15]. On the whole, these methods use a probabilistic means of connecting the initial configuration to the final configuration, enabling an improved capacity to handle uncertainty, a relative blindness to environmental complexity, and a capability to generate feasible solutions with minimal computational burden. Complexity increases with the incorporation of planning techniques to satisfy dynamic constraints and improve solution optimality; however, solution optimality is never guaranteed [15].

Nonlinear optimal control methods offer significant advantages to other approaches, namely the inherent satisfaction of vehicle and problem constraints and the intrinsic extremal nature of solutions. Generally, two distinct methods exist for solving the nonlinear optimal control problems [16-17], direct and indirect. Indirect methods make use of Pontryagin's maximum principle and create a two-point boundary value problem. Direct methods transfer the problem into a nonlinear programming problem by discretizing the trajectory and this problem can be solved by any one of a number of nonlinear optimization solvers. Typically direct methods are considered more numerically advantageous that indirect methods, but despite their differences, they all share the same concerns including: solution convergence, computational complexity, and the need for a good initial guess. Advances in computing power and improvement in optimization algorithms are changing that paradigm and research is showing the applicability of optimal control techniques in guidance and control

[18-21]. Whereas optimization methods traditionally created a solution in minutes to hours, solutions can now be found within seconds or less, and the improvements in computational speed increase their ability to handle problem uncertainty. Aerospace applications made use of optimal control solutions because the problems typically permitted the trajectories to be generated offline; now the improvements in optimal control methods present a strong argument for their application in online planners and with robotics problems.

2.0 SOLUTION APPROACH

Given the progress made in applying optimal control methods to online aerospace applications [18-19] and being aware of the ability to eliminate the associated computational burden [20, 22], this paper focuses on the application of these techniques to a new breed of problems, sharing attributes with both aerospace and robotics applications. This problem is that of the unmanned vehicle, characterized by a lack of global knowledge, complex obstacle-rich environments, and a need for feasible solutions in the face of uncertainty. On the other hand, these systems typically incorporate sophisticated sensors and ample computational power.

The research presented here evaluates and validates the concept of trajectory planning for unmanned vehicles with optimal control methods. Being a feasibility study, robustness is not proven, and while the concerns of uncertainty are currently being evaluated, those efforts are not discussed here. Instead, the primary thrust of this work is the optimization of kinematic trajectories within varying, complex environments. The optimization tool used during this exercise was DIDO©, a software package based on pseudospectral methods [1-6] that runs within the MATLAB environment.

3.0 THE OPTIMAL CONTROL PROBLEM

One of the many advantages to utilizing optimal control methods is the relative ease with which a multitude of problems is formulated. Any kinematic, dynamic, or path constraint or optimality criteria that is appropriately expressed in a mathematical manner can be rapidly incorporated into the problem formulation. This inherent portability and flexibility makes these techniques powerful, but the fundamental key is to express the characteristics appropriately. In this section, the UGV problem will be defined within the framework of an optimal control problem; all characteristics will be covered including the kinematic equations, path constraints, scaling, and necessary conditions. Even though the detailed focus remains on one version of an UGV, the specific equations are not as important as the validation of the method; due to generality of this method any system could be represented.

3.1 Unmanned Ground Vehicle

The term “unmanned ground vehicle” is generic; there are a multitude of systems that could fit that name. In an attempt to maintain generality, a common example is used – a four-wheeled car with rear-wheel drive and front-wheel steering. This system is well-studied, and the nonholonomic-nature of the constraints adds kinematic complexity. A simple, kinematic model of the car [8] is shown in Figure 1 and the state and control vectors are presented in Equations (1) and (2), respectively. The x-y location of the car represents the current position of the center point of the rear axle. The car’s orientation angle is measured with respect to the horizontal axis and is presented as the state variable theta. The steering angle, phi, is measured with respect to the car’s heading, or velocity vector, and the variable ‘L’ measures the distance between the front and rear axles.

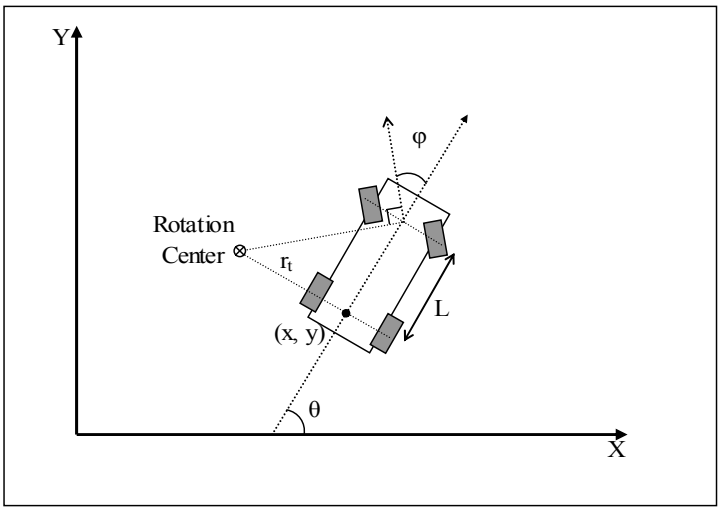

Figure 1: A four-wheel car model with front-wheeled steering.

$$\underline{x} = \begin{bmatrix} x \\ y \\ \theta \end{bmatrix} \tag{1}$$

$$\underline{u} = \begin{bmatrix} v \\ \phi \end{bmatrix} \quad where \quad \underline{u} \in \mathrm{U} = \begin{Bmatrix} v: & v_{\min} \le v(t) \le v_{\max} \\ \phi: & \phi_{\min} \le \phi(t) \le \phi_{\max} \end{Bmatrix} \tag{2}$$

The steering angle must be between ±90° for computational and for practical purposes it is typically much less than that. Unlike the Reeds-Shepp or Dubin's cars the velocity is allowed to change continuously between the extremes similarly to the capability of a real car.

Given this UGV characterization, Equation (3) shows the resulting nonlinear, kinematic equations and Equation (4) provides the vehicle's current turning radius.

$$\dot{\underline{x}} = \begin{bmatrix} v\cos\theta \\ v\sin\theta \\ \dfrac{v}{L}\tan\phi \end{bmatrix} \tag{3}$$

$$r_{t,\min} = \frac{L}{\tan\phi_{\max}} \tag{4}$$

3.2 Obstacle Representation

In general, a constraint can be a function of the state, control, or time so long as it is written mathematically. For the car problem, there exist vehicle constraints – holonomic kinematics and control constraints – and path constraints. The path constraints are the obstacles around which the car must maneuver. For simplicity and computational efficiency it was desirable to represent the path constraints as continuous, differentiable algebraic functions. With this framework in mind, the p-norm was used to create generic shapes including: diamonds, circles and ellipses, and squares and rectangles. Figure 2 demonstrates how the p-norm can be manipulated to create these obstacle shapes; the ellipse and rectangle are simply extensions of the circle and square respectively where the distance along the x and y axes are dissimilar. Equation (5) presents the common equation used to build these shapes. Any point outside the obstacles yields a path constraint value greater than zero. The square and rectangular shapes result from the infinity norm; however, during calculations, this is approximated by a large value for the exponent. Higher values for the exponent yielded sharper corners, but they often created numerical concerns. The square in Figure 2 was created by setting the exponent to 100.

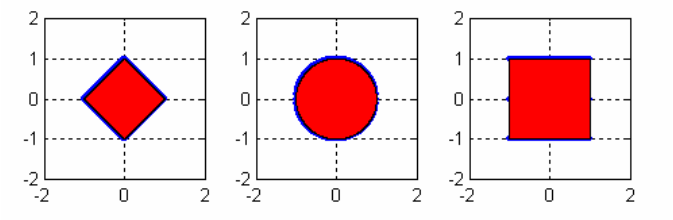

Figure 2: Unit p-norms for p = 1, 2, and infinity respectively.

$$h_i\left(x(t),y(t)\right)=\left(\frac{x(t)-x_c}{a}\right)^p+\left(\frac{y(t)-y_c}{b}\right)^p-c^p \qquad (5)$$

Modelling shapes outside of these basic geometries is a powerful option and, in most cases, more realistic of the random nature of the world. However, even simple polygonal shapes are non-trivial since they cannot be wholly described by one algebraic equation. Figure 3 is a straightforward example of a simple shape, described by the confluence of three lines, which cannot be characterized by the p-norm.

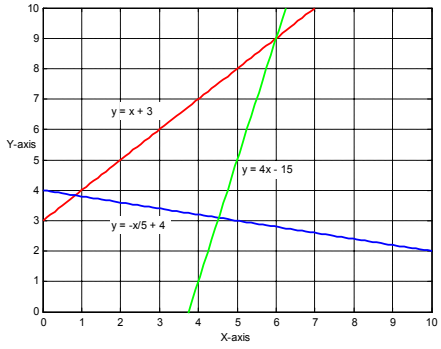

Figure 3: Simple polygonal constructed by three lines.

Using the equation for each line it is possible to create a series of inequality constraints that defines each point within the obstacle. This concept is evidenced by Equation Set (6).

$$\underline{g}(\underline{x}) = \begin{bmatrix} g_1(\underline{x}) \\ g_2(\underline{x}) \\ g_3(\underline{x}) \end{bmatrix} = \begin{bmatrix} -y + x + 3 \\ y + x/5 - 4 \\ y - 4x + 15 \end{bmatrix} > \underline{0} \tag{6}$$

While every point within the obstacle satisfies all of the three constraints, every point outside the obstacle must not satisfy at least one; this is a mathematical 'or' condition. Given that continuous and smooth functions are desirable for DIDO implementation, a simple logical operation could not be implemented. Instead, the resulting g vector must be searched for the minimum single value; if this value is less than zero, it can be stated that the point must lie outside the obstacle. From a mathematical perspective, every feasible point on the map in Figure 3 satisfies Equation (7).

$$h_i\left(x(t), y(t)\right) = \min\left\{g_1(\underline{x}), g_2(\underline{x}), g_3(\underline{x})\right\} < 0 \tag{7}$$

Figure 4 illustrates this concept. The left panel shows the mathematical constraints of the triangular obstacle and right panel shows the resulting values of the new path constraint function over the positional domain.

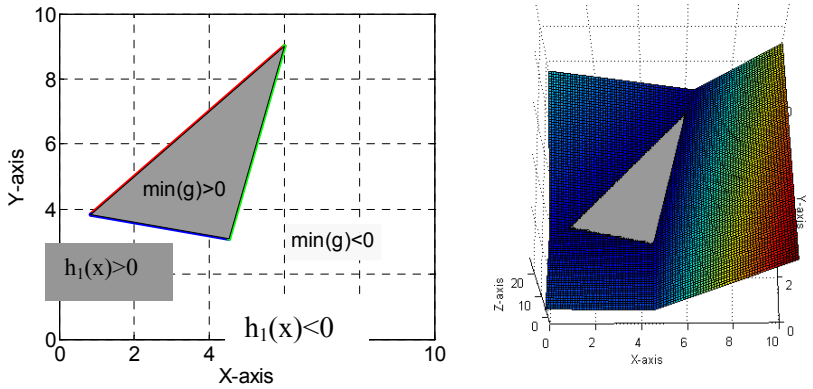

Figure 4: Non-smooth constraint representation of a simple polygonal shape.

The sharp corners are captured exactly with this technique. The result is continuous and grows linearly with distance from the obstacle; however, the result is not smooth, i.e. non-differentiable. The non-smoothness arrives from the fact that the path constraint is essentially the union of three planes. It is possible to correct the non-smoothness, but this comes at a loss of accuracy in rendering the sharp corners. Equation (8) displays the mathematical expression for the smooth polygonal constraint, and it occurs in three distinct steps.

$$h_{P,i}\left(x(t), y(t)\right) = \ln\left[\left(e^{-g_1(\underline{x})\cdot p} + e^{-g_2(\underline{x})\cdot p} + e^{-g_3(\underline{x})\cdot p}\right)^{1/p}\right] > 0 \tag{8}$$

In the first step, the elements of g are multiplied by negative one and placed into an exponent. This maps all previously positive values of g to numbers between zero and one and all previously negative values to

numbers greater than one. The next step is to take a p-norm; this step extracts the largest, single value of g. The last step uses the natural logarithm to scale the values back to the original range. In this case a positive value for the path constraint indicates a position outside the obstacle, illustrated in Table 1. Both the power of the p-norm and the base of the exponent/logarithm can be altered to provide better smoothness. Figure 5 provides a picture of the result; the loss of sharpness around the corners is visible. Without a precise representation of the obstacle's corners, it is necessary during implementation to add a small buffer around obstacles to ensure that the path produced is actually obstruction-free.

Table 1: Mapping of vehicle position to path constraint value.

	Inside Obstacle	On Obstacle	Outside Obstacle
$g(\underline{x})$	> 0	$= 0$	< 0
$-g(\underline{x})$	< 0	$= 0$	> 0
$e^{-g(\underline{x})}$	$[0,1]$	$= 1$	> 1
$\| e^{-g(\underline{x})} \|_p$	$[0,1]$	$= 1$	> 1
$\ln(\| e^{-g(\underline{x})} \|_p)$	< 0	$= 0$	> 0

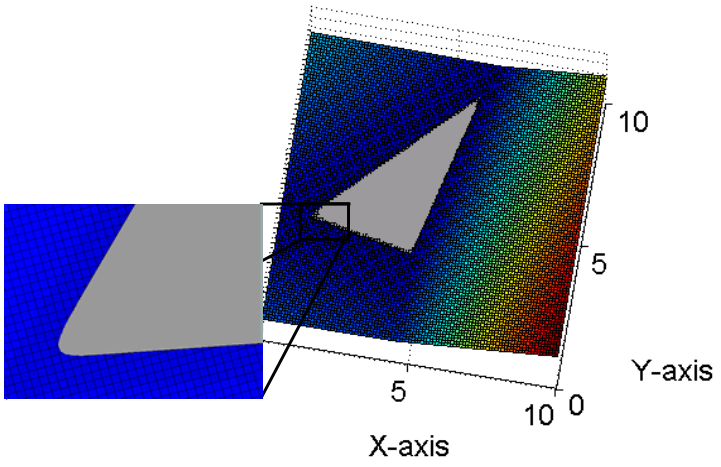

Figure 5: Smoothed constraint representation of a polygonal shape.

The p-norm and polygonal representations of obstacles can be used interchangeably or simultaneously during problem formulation. While the polygonal representation is more functional, it is slightly more complex to prepare.

3.3 Problem Formulation

After presenting the kinematic and path constraints, the optimal control problem can be stated mathematically. Conceptually, the problem is defined as the generation of a time-optimal trajectory that enables the UGV to travel from some initial condition to some final condition while satisfying the kinematic and path constraints. Before proceeding, it is important to remember that the optimal control problem is solved with a numerical optimization tool and for that reason good scaling is necessary [23]. With this in mind, Equation Set (9) shows the new scaled variables that will be used during the problem formulation – the scaling factor for each

variable is represented as the capitalized version of that variable letter and the scaled variable is denoted by the bar.

$$\underline{\bar{x}} = \begin{bmatrix} \bar{x} \\ \bar{y} \\ \bar{\theta} \end{bmatrix} = \begin{bmatrix} x/X \\ y/Y \\ \theta/\Theta \end{bmatrix} \qquad \underline{\bar{u}} = \begin{bmatrix} \bar{v} \\ \bar{\phi} \end{bmatrix} = \begin{bmatrix} v/V \\ \phi/\Phi \end{bmatrix} \qquad \bar{t} = t/T \tag{9}$$

If the scaling factors for the control variables are set to the maximum respective value, the optimal control problem can be represented mathematically as Equation Set 10.

$$\underline{\bar{x}} = \begin{bmatrix} \bar{x} \\ \bar{y} \\ \bar{\theta} \end{bmatrix} \in \bar{X} = R^3, \quad \underline{\bar{u}} \in \bar{U} := \begin{Bmatrix} \bar{v} : -1 \le \bar{v} \le 1 \\ \bar{\phi} : -1 \le \phi \le 1 \end{Bmatrix}$$

$$\textit{Minimize} \quad J\left[\underline{\bar{x}}(\cdot), \underline{\bar{u}}(\cdot), \bar{t}_f\right] = \bar{t}_f$$

$$\textit{Subject to} \quad \dot{\underline{\bar{x}}}(\bar{t}) = \begin{bmatrix} \bar{v} \cdot \cos\left(\Theta\bar{\theta}\right)\dfrac{V \cdot T}{X} \\ \bar{v} \cdot \sin\left(\Theta\bar{\theta}\right)\dfrac{V \cdot T}{Y} \\ \dfrac{\bar{v}}{L} \cdot \tan\left(\Phi\bar{\phi}\right)\dfrac{V \cdot T}{\Theta} \end{bmatrix}$$

$$\underline{\bar{x}}(t_0) = [\underline{0}] \tag{10}$$

$$\bar{t}_0 = 0$$

$$e\left(\underline{\bar{x}}_f, \bar{t}_f\right) = \begin{bmatrix} \bar{x}\left(\bar{t}_f\right) - \bar{x}_f \\ \bar{y}\left(\bar{t}_f\right) - \bar{y}_f \end{bmatrix} = [\underline{0}]$$

$$h_i(\bar{x}(\bar{t}), \bar{y}(\bar{t})) > 0$$

In this formulation, the initial condition includes the position and orientation while the endpoint condition includes only the position. If the final orientation of the vehicle is important, it could be included with little effort.

3.4 Optimality Conditions

Proving that the results of an optimal control problem are indeed globally optimal is intractable, but several criteria can be demonstrated to evidence the extremal nature of the solution. The criteria used within this research included satisfaction of the necessary conditions, verification of solution feasibility, and validation of Bellman's principle. Bellman's principle was validated by ensuring the concurrence of optimal sub-trajectories that begin and end on the originally defined solution. Feasibility is verified by propagating the

system kinematics from the initial condition using the calculated optimal control trajectory and MATLAB's Runge-Kutta algorithm. The necessary conditions for optimality, presented below, were verified, where possible, against the solution received from DIDO.

For the scaled problem introduced in the previous subsection, the control Hamiltonian can be written as Equation Set (11).

$$H\left(\underline{\bar{\lambda}},\underline{\bar{x}},\underline{\bar{u}},\bar{t}\right)=\underline{\bar{\lambda}}^{T}\cdot\begin{bmatrix}\bar{v}\cdot\cos\left(\Theta\bar{\theta}\right)\dfrac{V\cdot T}{X}\\ \bar{v}\cdot\sin\left(\Theta\bar{\theta}\right)\dfrac{V\cdot T}{Y}\\ \dfrac{\bar{v}}{L}\cdot\tan\left(\Phi\bar{\phi}\right)\dfrac{V\cdot T}{\Theta}\end{bmatrix} \qquad (11)$$
$$where\quad \underline{\bar{\lambda}}^{T}=\begin{bmatrix}\bar{\lambda}_{x} & \bar{\lambda}_{y} & \bar{\lambda}_{\theta}\end{bmatrix}$$

Using the Hamiltonian, the optimal control problem can be reformulated and presented as Equation (12).

$$\begin{aligned} &Minimize_{\underline{\bar{u}}} && H\left(\underline{\bar{\lambda}},\underline{\bar{x}},\underline{\bar{u}},\bar{t}\right)\\ &Subject\ to && \underline{\bar{u}}\in U\\ & && h_{i}\left(\bar{x}\left(\bar{t}\right),\bar{y}\left(\bar{t}\right)\right)>0\end{aligned} \qquad (12)$$

Equation (13) displays the resulting Lagrangian of the Hamiltonian.

$$\bar{H}\left(\underline{\bar{\mu}},\underline{\bar{\lambda}},\underline{\bar{x}},\underline{\bar{u}},\bar{t}\right)=\underline{\bar{\lambda}}^{T}\cdot\begin{bmatrix}\bar{v}\cdot\cos\left(\Theta\bar{\theta}\right)\dfrac{V\cdot T}{X}\\ \bar{v}\cdot\sin\left(\Theta\bar{\theta}\right)\dfrac{V\cdot T}{Y}\\ \dfrac{\bar{v}}{L}\cdot\tan\left(\Phi\bar{\phi}\right)\dfrac{V\cdot T}{\Theta}\end{bmatrix}+\underline{\bar{\mu}}^{T}\begin{bmatrix}\bar{v}\\ \bar{\phi}\\ \bar{h}\left(\bar{x}\left(\bar{t}\right),\bar{y}\left(\bar{t}\right)\right)\end{bmatrix} \qquad (13)$$
$$where\quad \underline{\bar{\mu}}^{T}=\begin{bmatrix}\bar{\mu}_{v} & \bar{\mu}_{\phi} & \bar{\mu}_{h}\end{bmatrix}$$

After creating the mathematical problem, it is possible to formulate the necessary conditions for optimality.

The first provision is the Hamiltonian Minimization Condition (HMC) and its affect is shown Equation (14).

$$\frac{\partial\bar{H}}{\partial\underline{\bar{u}}}=\begin{bmatrix}0\\0\end{bmatrix}=\begin{bmatrix}\bar{\lambda}_{x}\cdot\cos\left(\Theta\bar{\theta}\right)\cdot\dfrac{T\cdot V}{X}+\bar{\lambda}_{y}\cdot\sin\left(\Theta\bar{\theta}\right)\cdot\dfrac{T\cdot V}{Y}+\bar{\lambda}_{\theta}\cdot\tan\left(\Phi\bar{\phi}\right)\cdot\dfrac{T\cdot V}{L\cdot\Theta}+\bar{\mu}_{v}\\ \bar{\lambda}_{\theta}\cdot\bar{v}\cdot\sec^{2}\left(\Phi\bar{\phi}\right)\cdot\dfrac{T\cdot\Phi}{L\cdot\Theta}+\bar{\mu}_{\phi}\end{bmatrix} \qquad (14)$$

Complementing this result is the Karush-Kuhn-Tucker (KKT) conditions for the control and path covectors.

$$\bar{\mu}_v \begin{cases} \leq 0 & \\ = 0 & for \quad -1 < \bar{v}(\bar{t}) < 1 \\ \geq 0 & \end{cases} \begin{matrix} \\ \bar{v}(\bar{t}) = -1 \\ \\ \bar{v}(\bar{t}) = 1 \end{matrix}$$

$$\bar{\mu}_\phi \begin{cases} \leq 0 & \\ = 0 & for \quad -1 < \bar{\phi}(\bar{t}) < 1 \\ \geq 0 & \end{cases} \begin{matrix} \\ \bar{\phi}(\bar{t}) = -1 \\ \\ \bar{\phi}(\bar{t}) = 1 \end{matrix} \tag{15}$$

$$\bar{\mu}_h \begin{cases} = 0 & for \quad h_i\left(\bar{x}(\bar{t}), \bar{y}(\bar{t})\right) > 0 \\ \leq 0 & \quad\quad h_i\left(\bar{x}(\bar{t}), \bar{y}(\bar{t})\right) = 0 \end{cases}$$

Given the time optimality of the trajectory, it is expected that Equation (16) be true.

$$\bar{\mu}_v \geq 0 \qquad and \qquad \bar{\mu}_\phi = 0 \tag{16}$$

The first condition corresponds to a maximum vehicle velocity, and the second corresponds to steering angle between the extremes. Using these predictions little can be said for the first equation of the HMC; however, the first term in the second equation must be zero to satisfy optimality conditions when non-extremal steering values are indicated. This can only occur if Equation (17) is true when the car is in motion.

$$\bar{\lambda}_\theta = 0 \tag{17}$$

The Adjoint Equation, Equation (18), describes the change of the costates over time.

$$\dot{\underline{\bar{\lambda}}} = \begin{bmatrix} \dot{\lambda}_x \\ \dot{\lambda}_y \\ \dot{\lambda}_\theta \end{bmatrix} = -\frac{\partial \bar{H}}{\partial \underline{\bar{x}}} = \begin{bmatrix} \bar{\mu}_{h,i} \cdot \dfrac{\partial h_i}{\partial \bar{x}} + \bar{\mu}_{h,i+1} \cdot \dfrac{\partial h_{i+1}}{\partial \bar{x}} + \ldots \\ \bar{\mu}_{h,i} \cdot \dfrac{\partial h_i}{\partial \bar{y}} + \bar{\mu}_{h,i+1} \cdot \dfrac{\partial h_{i+1}}{\partial \bar{y}} + \ldots \\ -\bar{\lambda}_x \cdot v \cdot \sin\left(\Theta\bar{\theta}\right) \cdot \dfrac{T \cdot V \cdot \Theta}{X} + \bar{\lambda}_y \cdot v \cdot \cos\left(\Theta\bar{\theta}\right) \cdot \dfrac{T \cdot V \cdot \Theta}{Y} \end{bmatrix} \tag{18}$$

From this equation and the KKT conditions, it can be deduced that $\bar{\lambda}_x$ and $\bar{\lambda}_y$ will remain constant whenever the vehicle is not touching an obstacle.

The Terminal Transversality Condition (TTC), Equation (19), provides boundary condition information on the costates. In this equation, $\bar{E}\left(\underline{\bar{v}}, \underline{\bar{x}}_f, \bar{t}_f\right)$ is the Endpoint Lagrangian and $E\left(\underline{\bar{x}}_f, \bar{t}_f\right)$ is the Endpoint Cost. Applying this condition to the car problem yields Equation (20), and it reveals the fact that Equation (17) must be true at the final time.

$$\underline{\bar{\lambda}}\left(\bar{t}_f\right)=\frac{\partial \bar{E}}{\partial \underline{\bar{x}}_f} \quad where \quad \bar{E}\left(\underline{\bar{\nu}},\underline{\bar{x}}_f,\bar{t}_f\right)=E\left(\underline{\bar{x}}_f,\bar{t}_f\right)+\underline{\bar{\nu}}^T e\left(\underline{\bar{x}}_f,\bar{t}_f\right) \quad and \quad \underline{\bar{\nu}}^T=\begin{bmatrix}\bar{\nu}_x & \bar{\nu}_y & \bar{\nu}_\theta\end{bmatrix} \tag{19}$$

$$\bar{E}\left(\underline{\bar{\nu}},\underline{\bar{x}}_f,\bar{t}_f\right)=\bar{t}_f+\underline{\bar{\nu}}^T\begin{bmatrix}\bar{x}\left(\bar{t}_f\right)-\bar{x}_f\\ \bar{y}\left(\bar{t}_f\right)-\bar{y}_f\end{bmatrix}$$

$$\underline{\bar{\lambda}}\left(\bar{t}_f\right)=\begin{bmatrix}\bar{\lambda}_x\left(\bar{t}_f\right)\\ \bar{\lambda}_y\left(\bar{t}_f\right)\\ \bar{\lambda}_\theta\left(\bar{t}_f\right)\end{bmatrix}=\begin{bmatrix}\bar{\nu}_x\\ \bar{\nu}_y\\ 0\end{bmatrix} \tag{20}$$

The final two necessary conditions pertain to the value of the Hamiltonian. The first is the Hamiltonian Value Condition (HVC), Equation (21), which is applied in situations, such as this, where the final time is not fixed.

$$\bar{H}\left(\bar{t}_f\right)+\frac{\partial \bar{E}}{\partial \bar{t}_f}=0 \quad \Rightarrow \quad \bar{H}\left(\bar{t}_f\right)=^- 1 \tag{21}$$

This result is complemented by the Hamiltonian Evolution Equation (HEE), Equation (22), which describes the time-evolution of the Hamiltonian value.

$$\dot{\bar{H}}=\frac{\partial \bar{H}}{\partial t} \quad \Rightarrow \quad \dot{\bar{H}}=0 \tag{22}$$

Together these two outcomes show that the value of the Hamiltonian must be a constant negative one throughout the trajectory.

In summary, these aforementioned conditions, alongside the feasibility verification and Bellman's principle validation, cannot prove global optimality, but they provide a demonstration of the extremal nature of the DIDO generated solution. In the very least, the existence of a feasible solution alone permits maneuver completion, a necessity for the unmanned vehicle application.

4.0 RESULTS

The results of this work are presented in two subsections. First, a basic problem is presented such that the optimality conditions can be analyzed. The more intricate problems that follow include only results. The entire data is not included only for the purposes of brevity.

4.1 Meeting the Optimality Conditions

A simple, three-circle problem was evaluated for the purposes of displaying the feasibility and optimality of this solution approach. In the X-Y coordinate frame, the vehicle is intended to travel from the location (0, 0)

and oriented down the X-axis to the location (10, 10). The optimal, vehicle state trajectory, as created in DIDO, is shown in Figure 6 and Figure 7. There is a noticeable distance between the vehicle trajectory and the side of the obstacle; the reason for this separation is in accounting for the size of the UGV.

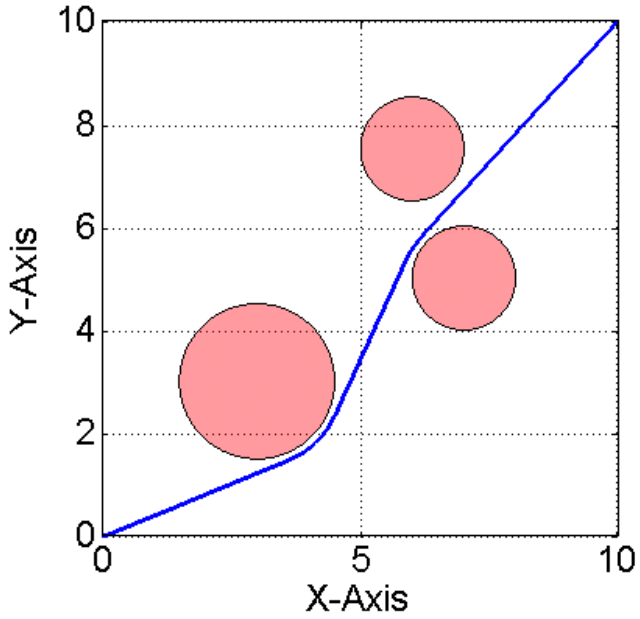

Figure 6: Time-optimal UGV trajectory through three circular obstacles.

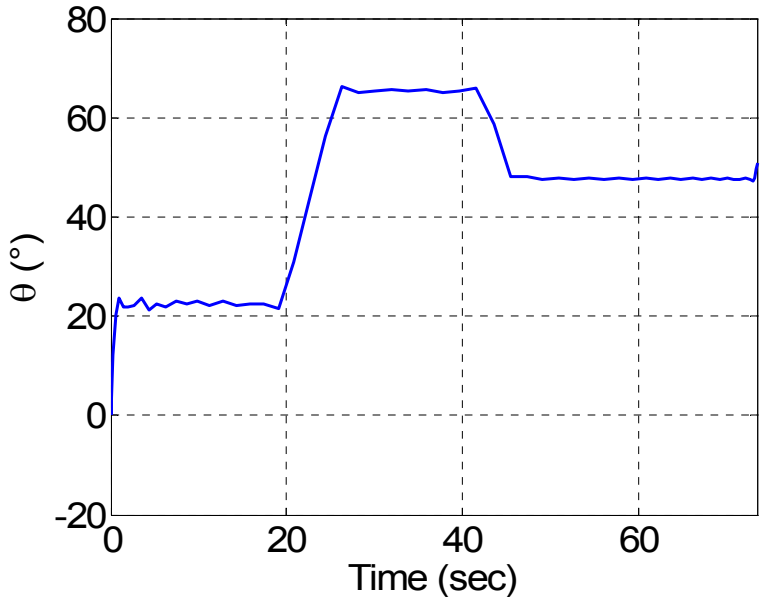

Figure 7: UGV orientation during time-optimal trajectory.

The UGV trajectory is straight unless it is maneuvering to avoid an obstacle, thus displaying the optimal nature of the result. The optimal control trajectory that generated this state path is shown in Figure 8. Using this control trajectory to test the feasibility of the solution, Figure 9 shows the comparison of the propagated and DIDO-generated states. The propagated and DIDO-generated states are identical; this indicates solution feasibility.

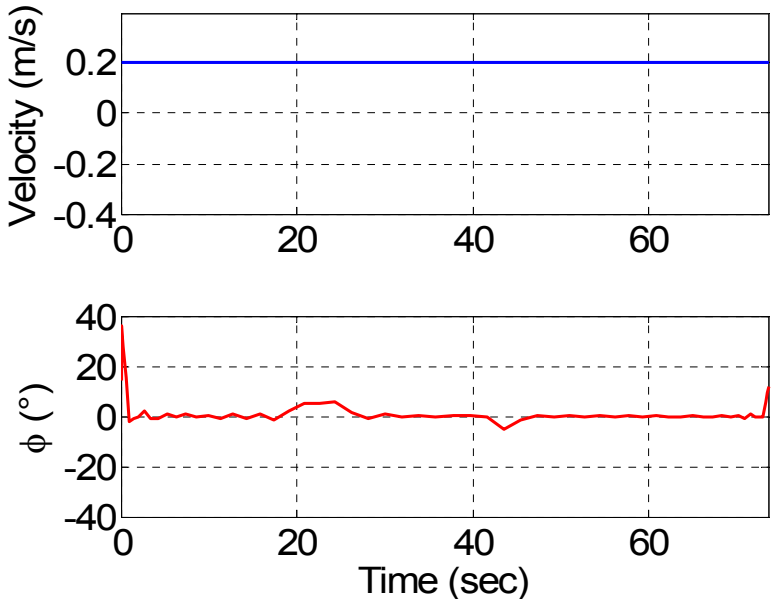

Figure 8: UGV time-optimal, control trajectory.

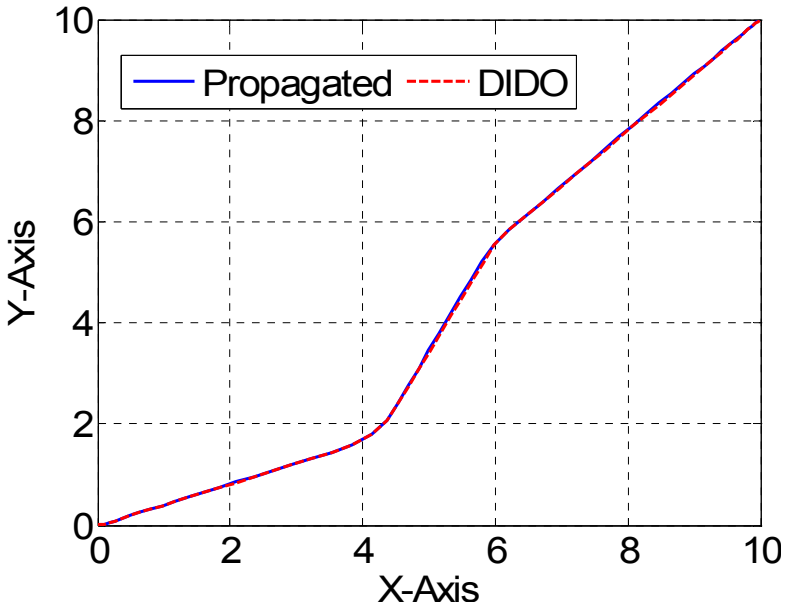

Figure 9: Feasibility verification of time optimal control trajectory.

The next several figures present elements of the necessary conditions. Figure 10 displays the value of the Hamiltonian throughout the trajectory; this result verifies Equation (21) and Equation (22). Figure 11 displays the confirmation of Equation (14), the Hamiltonian Minimization Condition, where the partial derivative of the Hamiltonian with respect to each control variable should be equal to zero. The results display some numerical error, but this is minimal and does not distract from the feasibility of the solution.

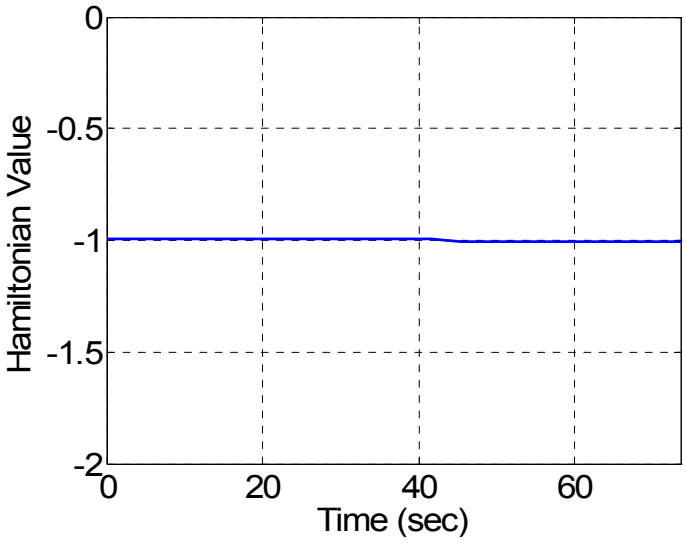

Figure 10: Evolution of Hamiltonian value during time-optimal trajectory.

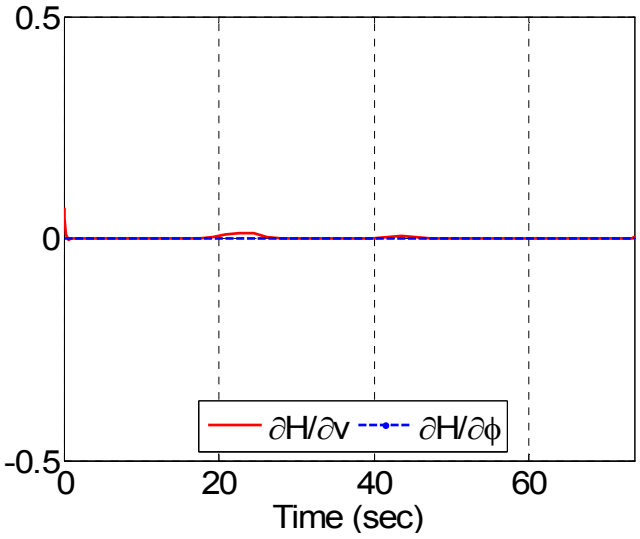

Figure 11: Verification of Hamiltonian Minimization Condition.

Figure 12 presents the costates and shows that Equation (17) is true, i.e. λ_θ equals zero. Figure 13 shows the path constraint covectors, and in accordance with the KKT conditions, the covectors are only active while the vehicle is touching a path constraint. Analyzing Figure 13 alongside Figure 12, it is apparent that Equation (18) is proven; namely, λ_x and λ_y are constant unless the vehicle is touching an obstacle.

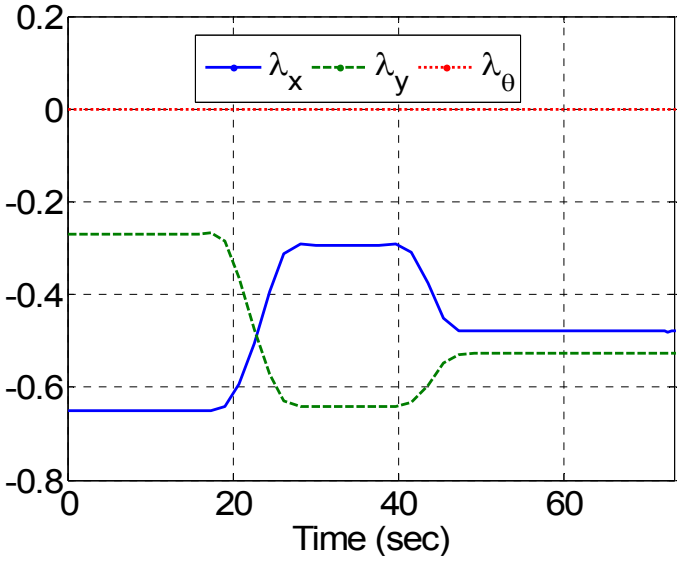

Figure 12: Costate values during time-optimal trajectory.

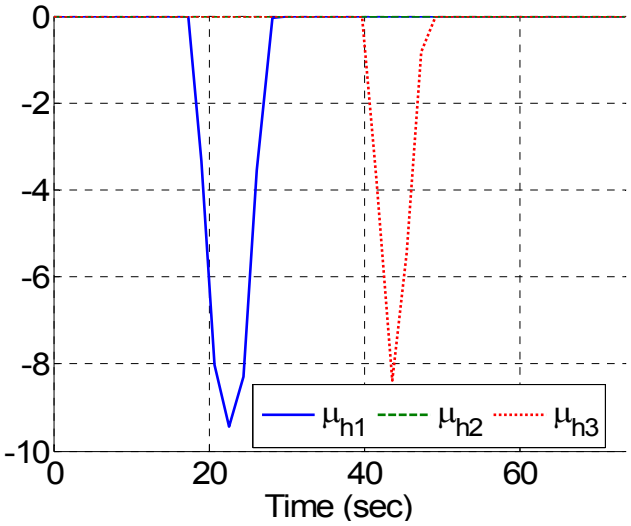

Figure 13: Path constraint covector values during time-optimal trajectory.

The last necessary condition is the KKT condition associated with the control variables. The maximum velocity is used throughout the trajectory and for that reason it maintains a positive value. Similarly, a non-maximum value of the steering angle is used and it maintains a value of zero.

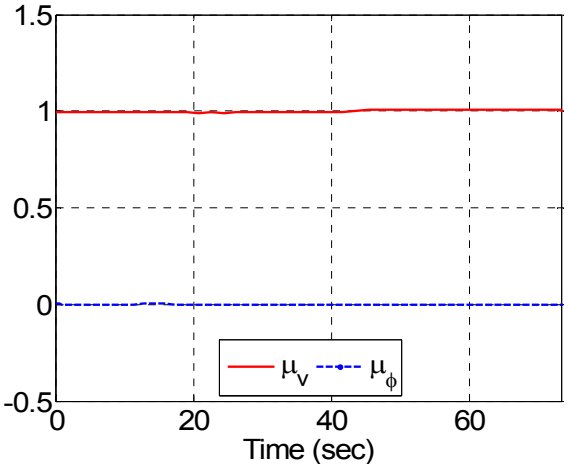

Figure 14: Control constraint covector values during time-optimal trajectory.

The remaining condition of optimality is Bellman's principle. In this experiment, Bellman's principle is validated by comparing three optimal sub-trajectories to the original optimal solution. These sub-trajectories begin along the original trajectory at the one-third, one-half, and two-thirds distance locations as shown in Figure 15. Figure 15 illustrates the fact that all three sub-trajectories are coincident with the original time-optimal trajectory and Figure 16 illustrates the fact that the maneuver cost is consistent across each trajectory. This provides further evidence to the extremal nature of the DIDO-generated solution.

In summary, the results shown above display the agreement of the DIDO generated solution with the conditions of optimality. The global optimality of the solution is not guaranteed; however the solution is proven feasible and the extremal nature is verified.

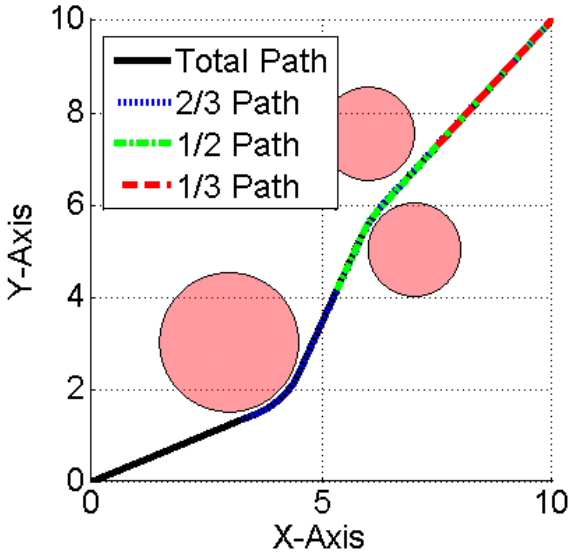

Figure 15: Validation of solution optimality with Bellman's principle.

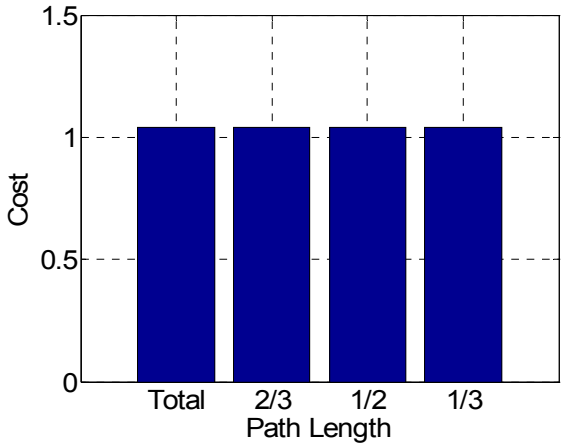

Figure 16: Validation of optimal cost with Bellman's principle.

4.2 Extended Applications

Having shown the validity of this solution approach, this subsection focuses on the illustration of its practicality and applicability by implementing this approach with various problems.

4.21 Various Obstacle Shapes

Section 3.2 introduced the concepts used to mathematically represent the various obstacle shapes that can be incorporated into the optimal control problem. Those concepts are incorporated below to evidence their applicability. Figure 17 shows a time-optimal trajectory generated against a multi-shape obstacle environment, including squares, diamonds, rectangles, circles, and ellipses. The result displays similar characteristics to the three-circle problem; specifically, the vehicle travels in straight lines except under the situation of touching an obstacle.

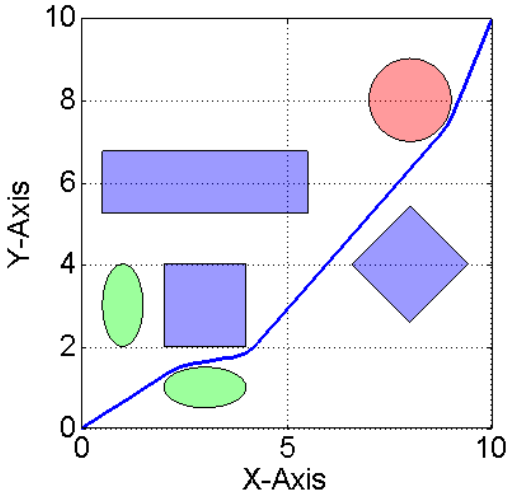

Figure 17: Time-optimal trajectory versus multi-shape obstacle environment.

Figure 18 illustrates the capability of this technique against a polygonal obstacle shape. In this particular instance, a random, five-sided obstacle is incorporated.

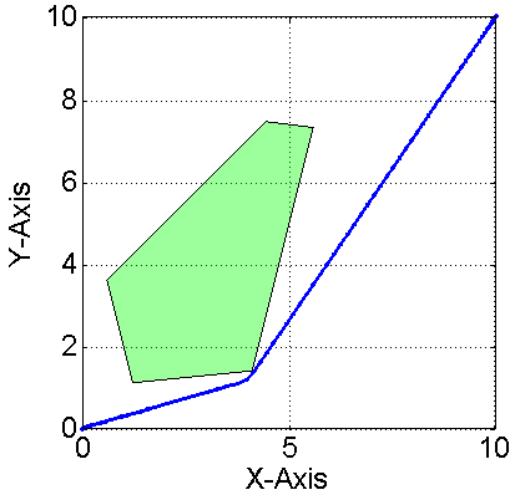

Figure 18: Time-optimal trajectory versus polygonal shape obstacle.

4.22 Obstacle Rich Environment

In the previous examples, the usefulness of optimal control techniques versus various obstacle shapes was evidenced, but relatively few obstacles were incorporated into each environment. Figure 19 evidences optimal control techniques against a 32-obstacle environment with circular obstacles.

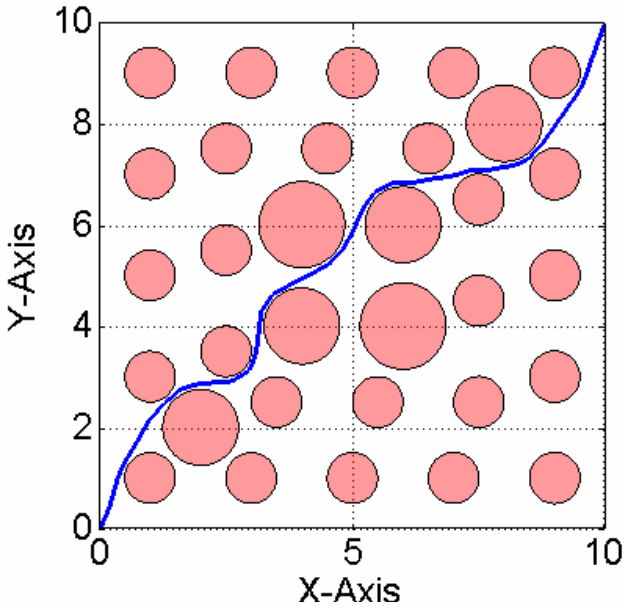

Figure 19: Time-optimal trajectory versus obstacle rich environment.

4.24 Control Failure

The previous examples show that optimal control techniques are successful in various, complex environments, but the problem in this subsection tests the ability to find a solution in the event of UGV damage. Figure 24 shows the optimal control trajectory when the vehicle must turn left, i.e. the minimum and maximum steering angle values are positive. In this situation, the solution is not initially intuitive or well understood. The time-optimal result requires two types of motion. The first type combines forward motion of the vehicle with a minimum steering angle; this results in a maximum turning radius. The second type of motion combines the backward motion of the vehicle with a maximum steering angle; this results in a minimum turning radius. In total, the UGV moves forward with a minimum turning radius and then backward with the maximum turning radius to align for the next forward motion. This type of motion is used in a repetitive fashion in Figure 24 to successfully navigate the obstacles.

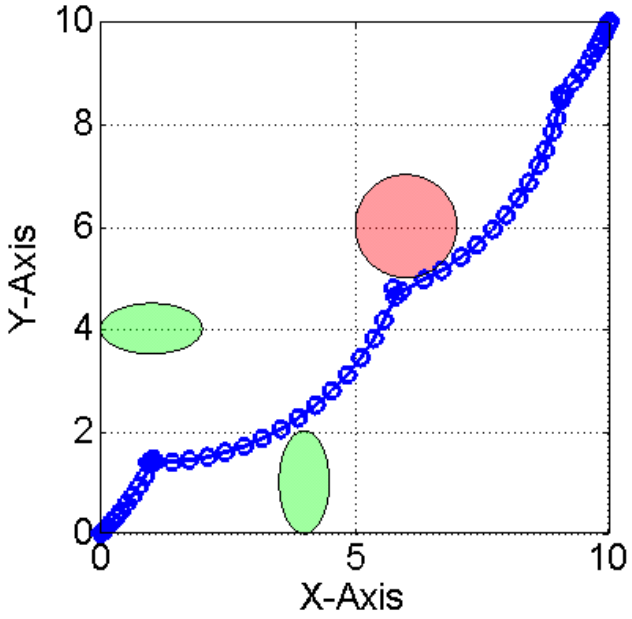

Figure 24: Time-optimal maneuver where the vehicle suffers a control failure.

4.25 Dynamic Environments

Many real-world problems involve dynamic environments, where either the destination or obstacles are moving, and examples of this would be typical highway travel and a vehicle interceptor mission, respectively. These problems require significant knowledge about the obstacles and targets in their environment, but with good sensors and positional knowledge, these assumptions are not unrealistic. For example, in the case of an aircraft carrier landing, the airplane could easily know accurate locations of itself and the target. Figure 25 shows the problem of a moving destination or target with two circular obstacles along the path. The results are displayed as an image generated from a strobe light so that the entire maneuver is visible within one frame. Throughout the trajectory, the vehicle does not drive towards the instantaneous location of the target; it drives towards the final location of the target. This allows the trajectory to be optimal.

The second experiment involves two, circular obstacles moving at different speeds and a stationary destination. Figure 26 displays these results. In this situation, a strobe image is confusing; therefore, the

results are displayed as movie frame scenes. From Figure 26 it is visible that the vehicle reaches the destination without hitting the obstacles; however, the vehicle's trajectory is within close proximity of the obstacles, a visual indication of optimality.

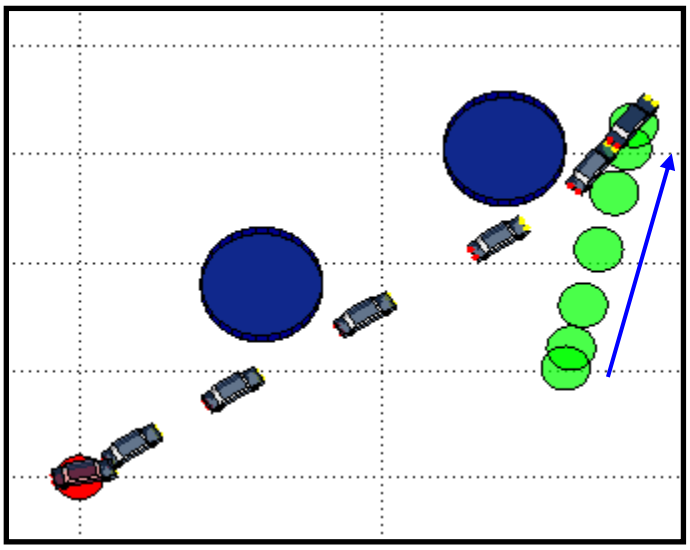

Figure 25: Time-optimal maneuver toward a moving target (strobe image).

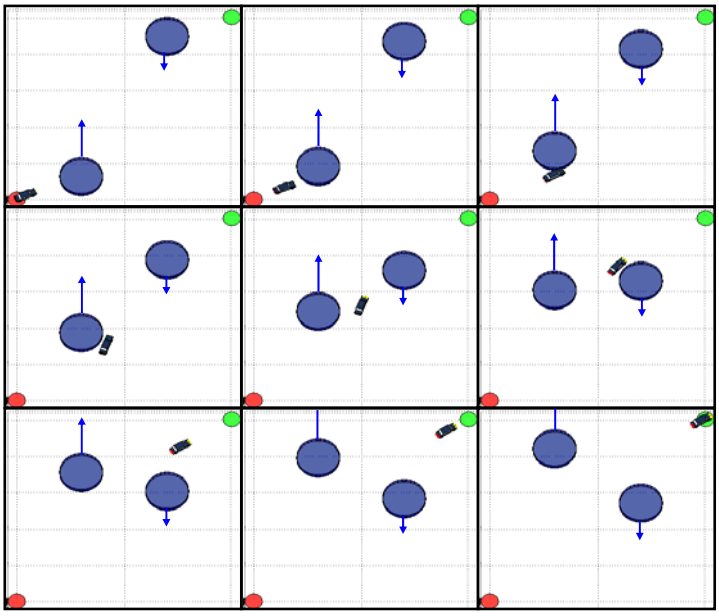

Figure 26: Scenes from a time-optimal maneuver around moving obstacles.

5.0 REFERENCES

[1] Gong, Q., Kang, W. and Ross, I. M., "A Pseudospectral Method for the Optimal Control of Constrained Feedback Linearizable Systems," *IEEE Transactions on Automatic Control*, Vol. 51, No.7, July 2006, pp.1115-1129.

[2] Ross, I. M. and Fahroo, F., "Issues in the Real-Time Computation of Optimal Control," *Mathematical and Computer Modelling*, An International Journal, Vol. 43, Issues 9-10, May 2006, pp.1172-1188. (Special Issue: Optimization and Control for Military Applications).

[3] Ross, I. M. and Fahroo, F., "Legendre Pseudospectral Approximations of Optimal Control Problems," *Lecture Notes in Control and Information Sciences,* Vol. 295, Springer-Verlag, New York, 2003, pp 327-342.

[4] Ross, I. M. and D'Souza, C. N., "A Hybrid Optimal Control Framework for Mission Planning," *Journal of Guidance, Control and Dynamics*, Vol. 28, No. 4, July-August 2005, pp.686-697.

[5] Ross, I. M. and Fahroo, F., "Pseudospectral Methods for the Optimal Motion Planning of Differentially Flat Systems," *IEEE Transactions on Automatic Control*, Vol.49, No.8, pp.1410-1413, August 2004.

[6] Ross, I. M. and Fahroo, F., "Pseudospectral Knotting Methods for Solving Optimal Control Problems," *Journal of Guidance, Control and Dynamics*, Vol. 27, No. 3, pp.397-405, 2004.

[7] LaValle, S. M., *Planning Algorithms*, Cambridge University Press, 2006.

[8] Choset, H. et al., *Principles of Robot Motion; Theory, Algorithms, and Implementation*, The MIT Press, 2005.

[9] Khatib, O., "Real-time Obstacle Avoidance for Manipulators and Mobile Robots," *International Journal for Robotics Research*, v.5, no.1, pp. 90-99, 1986.

[10] Barraquand, J., Langlois, B., and Latombe, J., "Numerical Potential Field Techniques for Robot Path Planning," *IEEE Transactions on Systems, Man, and Cybernetics*, v. 22, no. 2, March/April 1992.

[11] Shimoda, S., Kuroda, Y., and Iagnemma, K., "Potential Field Navigation of High Speed Unmanned Ground Vehicles on Uneven Terrain," paper presented at the International Conference on Robotics and Automation, Barcelona, Spain, April 2005.

[12] Zefran, M., *Continuous Methods for Motion Planning*, Doctoral Dissertation, pp. 1-14, University of Pennsylvania, December 1996.

[13] LaValle, S.M. and Kuffner, J.J., "Randomized Kinodynamic Planning," *International Journal of Robotics Research*," v. 20, no. 5, May 2001.

[14] Kavraki, L.E., Latombe, J.C., Svestka, P., and Overmars, M.H., "Probabilistic Roadmaps for Path Planning in High-dimensional Configuration Spaces," *IEEE Tranactions on Robotics and Automation*, v. 12, no. 4, June 1996.

[15] LaValle, S.M., "From Dynamic Programming to RRTs: Algorithmic Design of Feasible Trajectories," *Control Problems in Robotics*, pp. 19-37, Springer-Verlag, Berlin, 2002.

[16] Ross, I. M. and Fahroo, F., "A Perspective on Methods for Trajectory Optimization," *Invited Paper*, *Proceedings of the AIAA/AAS Astrodynamics Conference*, AIAA-2002-4727, Monterey, CA, 5-8 August 2002.

[17] Betts, J.T., "Survey of Numerical Methods for Trajectory Optimization," *AIAA Journal of Guidance, Control, and Dynamics*, v. 21, no. 2, pp. 193-207, March-April 1998.

[18] Sekhavat, P., Fleming, A., and Ross, I.M., "Time-Optimal Nonlinear Feedback Control for the NPSAT1 Spacecraft," *Proceedings of the 2005 IEEE/ASME International Conference on Advanced Intelligent Mechatronics*, Monterey, CA, 24-28 July 2005.

[19] Bollino, K., Ross, I.M., and Doman, D., "Optimal Nonlinear Feedback Guidance for Reentry Vehicles," *AIAA Guidance, Navigation, and Control Conference*, Keystone, CO, 2006.

[20] Ross, I.M. and Fahroo, F., "Issues in the Real-Time Computation of Optimal Control," *Mathematical and Computer Modeling*, Pergamon Publication, 2005.

[21] Lewis, L.R., *Rapid Motion Planning and Autonomous Obstacle Avoidance for Unmanned Vehicles*, Master's Thesis, Naval Postgraduate School, December 2006.

[22] Moon, R.L., "Migration of a Real-Time Optimal Control Algorithm: From MATLAB to Field Programmable Gate Array," Master's Thesis, Naval Postgraduate School, Monterey, CA, December 2005.

[23] Ross, I.M., *Lecture Notes in Control and Optimization*, Naval Postgraduate School, Monterey, CA, 1998.

[24] Ross, I.M., Gong, Q., and Sekhavat, P., "Low-Thrust, High-Accuracy Trajectory Optimization," *Journal of Guidance, Control, and Dynamics*, 2006.

[25] Strizzi, J., Ross, I.M., and Fahroo, F., "Towards Real-Time Computation of Optimal Controls for Nonlinear Systems," *Proceedings of the 2002 AIAA Guidance, Navigation, and Control Conference*, AIAA Paper No. 2002-4945, August 2002.

[26] General Atomics Aeronautical Systems, "Aircraft Platforms: Altair," [http://www.ga-asi.com/products/index.php], 26 October 2006.